Effect of Hydrogen Bonding on Barrier-Free Proton Transfer in Anionic Complexes of Uracil with Weak Acids: $(U\ldots HCN)^-$ versus $(U\ldots H_2S)^-$

MACIEJ HARAŃCZYK,[a,b] JANUSZ RAK,[b] MACIEJ GUTOWSKI,[a,*] DUNJA RADISIC,[c] SARAH T. STOKES,[c] AND KIT H. BOWEN, JR.[c,*]

[a]Chemical Sciences Division, Pacific Northwest National Labolatory, 902 Battelle Boulevard, Richland, Washington 99352, USA

[b]Department of Chemistry, University of Gdansk, Sobieskiego 18, 80-952 Gdansk, Poland

[c]Department of Chemistry, Johns Hopkins University, Baltimore, Maryland 21218, USA

(Received 3 November 2003 and in revised form 18 November 2003)

Abstract. A photoelectron spectrum is reported for an anionic complex of uracil (U) with HCN. The effects of electron attachment to a complex of U with HA (A = CN, NC) have been studied at the density functional theory level with 6–31++G** basis sets and the B3LYP and MPW1K exchange correlation functionals. Critical anionic structures have been reexamined at the MP2/6–31++G** level. The B3LYP gas-phase deprotonation enthalpies are equal to 14.56, 15.13, and 15.12 eV for HNC, HCN, and H_2S, respectively. The experimental deprotonation enthalpies are 15.217 ± 0.009 and 15.212 ± 0.126 eV for HCN and H_2S, respectively. Hence, HCN and H_2S have very indeed similar deprotonation enthalpies. The photoelectron spectra of anionic complexes of uracil with HCN and H_2S are, however, very different. The $(UHCN)^-$ spectrum reveals a broad feature with a maximum between 1.2–1.4 eV, whereas the main feature of the $(UH_2S)^-$ spectrum has a maximum between 1.7 and 2.1 eV. We suggest that barrier-free proton transfer (BFPT) occurs in the $(UH_2S)^-$complex, but not in $(UHCN)^-$. Critical factors for the occurrence of BFPT have been analyzed. The difference between the $(UHCN)^-$ and $(UH_2S)^-$ complexes is attributed to differences in hydrogen bonds formed by HCN and H_2S with uracil.

1. INTRODUCTION

DNA is responsible for storage and processing of genetic information. The mutagenic properties of ionizing radiation have been well documented throughout the last century. Only a small percentage of the total DNA damage is due to the direct interaction of high-energy particles with genetic material.[1] These are the products of interaction of ionizing radiation with cellular environment that are the main mutagenic agents. The OH and H radicals, as well as secondary low-energy electrons are among the most abundant reactive species formed by radiolysis of water. While the connection between the presence of free radicals and the formation of DNA mutations is well characterized,[2,3] the role of low-energy electrons in genotoxicity has only recently been systematically addressed.[4,5] Recent reports indicate that around one-third of all DNA damage is induced by the interaction between this biopolymer and charged low-energy particles.[1,6]

The recent experiments by Sanche and coworkers[4,5] suggest that electrons with energies in a range of 1–20 eV can induce DNA damage. However, in contrast to the reactions between genetic material and reactive species such as free radicals and alkylating and oxidizing agents, low-energy electrons lead directly to single and double DNA strand breaks. The resonance structure of the damage quantum-yield versus incident electron energy suggests that the process proceeds via anionic states, probably localized on the nucleic acid bases. Such a mechanism of a single-strand break has been computationally studied by Barrios et al., who suggested that a barrier of 13 kcal/mol would have to be

*Authors to whom correspondence should be addressed. E-mails: maciej.gutowski@pnl.gov; kitbowen@jhu.edu

overcome to create a sugar–phosphate C–O-bond rupture initiated by an excess electron attachment to a DNA base.[7]

Negatively charged clusters of biologically important molecules have been extensively studied, both experimentally and theoretically.[8–10] The possibility[11–19] of electron localization on nucleic acid bases (NABs) has been an important topic throughout the years. It was suggested that NABs support valence anionic states. However, electronic stability of these states requires stabilization through the environment,[9] as isolated gas-phase species have not yet been determined. Only about ten years ago, noting large dipole moments of NABs, it was realized that the dipole-bound anions must also exist.[11] Our CCSD(T) results indicate that the valence anionic state of uracil (U) is vertically stable with respect to the neutral by 0.507 eV;[20] we also find the valence anionic state to be thermodynamically unstable by 0.215 eV with respect to the dipole-bound anionic state and by 0.147 eV with respect to the neutral. The current view is that valence anionic states remain unbound (or at best very weakly bound) for isolated NABs, but that they become dominant species upon solvation.[19,21]

Intra- and intermolecular tautomerizations involving nucleic acid bases have long been suggested as critical steps in mutations of DNA.[22–24] Intramolecular proton transfer reactions have been studied for gas-phase and hydrated nucleic acid bases.[24,25] The single and double proton transfers have been studied for ground- and excited-electronic states of nucleic acid base pairs.[22–34] The proton transfer reactions in the GC system have been found favorable for anions and unfavorable for the cation. Small kinetic barriers were reported for the latter reaction.

Recently we described a tautomerization process that occurs in complexes of uracil with proton donors, such as glycine, H_2S,[35] alanine,[36] and formic acid.[37] Denoting a proton donor as HA, the following process was identified:

$$U\cdots HA + e^- \rightarrow UH^{\cdot}\cdots A^- \qquad (1)$$

Our ab initio calculations and photoelectron spectroscopic measurements (PES) strongly suggested that the electron attachment to complexes of uracil with these HAs leads to a barrier-free proton transfer (BFPT) from the acid (HA) to the O8 atom of U, with the products being a neutral radical of hydrogenated uracil ($UH^{\cdot}$) and A^-. A driving force for the proton transfer is to stabilize the excess electron on a π^* orbital of the anionic base (see Fig. 1 for the numbering of atoms in uracil and the excess electron orbital in its valence π^* anionic state).

BFPT (or proton transfer with a low kinetic barrier) induced by electron attachment may also take place in DNA. To elucidate the fate of primary anionic states generated in DNA through irradiation with low-energy electrons, one therefore needs to determine factors governing the occurrence of proton transfer in complexes between anionic NABs and proton donors.

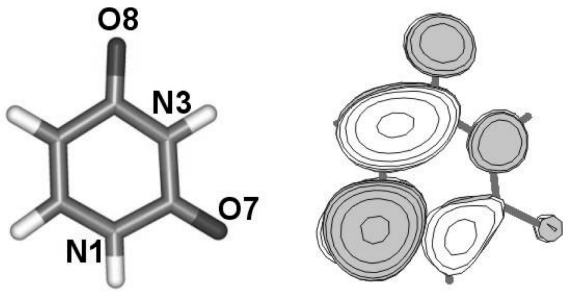

Fig. 1. Numbering of atoms in uracil (*left*) and the singly-occupied orbital for the anion of uracil in the valence π^* electronic state (*right*).

In a previous study we investigated anionic complexes of uracil with H_2A acids (A = O, S, Se),[35] and we discussed the occurrence of BFPT as an outcome of the interplay between the deprotonation energy of a proton donor and the protonation energy of the anionic uracil. These complexes formed cyclic structures (see Fig. 2 a), in which HA acts as a proton donor and a lone electron pair of A as a proton acceptor. The values of deprotonation enthalpy of H_2A changed by 2.1 eV across the A = O, S, Se series, and BFPT was predicted for A = S and Se, but not for A = O.

In the current study we concentrate on two weak acids that are characterized by very similar values of deprotonation enthalpy, but form different hydrogen bonds with uracil. These are HCN and H_2S, with an experimental deprotonation enthalpy of 15.217 ± 0.009[38] and 15.212 ± 0.126[39] eV, respectively. The former, being a linear triatiomic molecule, forms only one strong hydrogen bond with uracil. The latter, as mentioned above, forms two hydrogen bonds, resulting in a cyclic structure. The purpose of the current study is to explore whether the character of hydrogen bonding plays a role in the process of intermolecular proton transfer in anionic complexes of uracil. A replacement of HCN by its rare, more acidic, but still linear tautomer, HNC, provides further information about the factors controlling BFPT.

We report here a photoelectron spectrum of $(UHCN)^-$, which is compared with those of anions of (UH_2O) and (UH_2S) and interpreted on the basis of quantum chemical calculations for the neutral and anionic complexes. The $(UHCN)^-$ spectrum reveals a

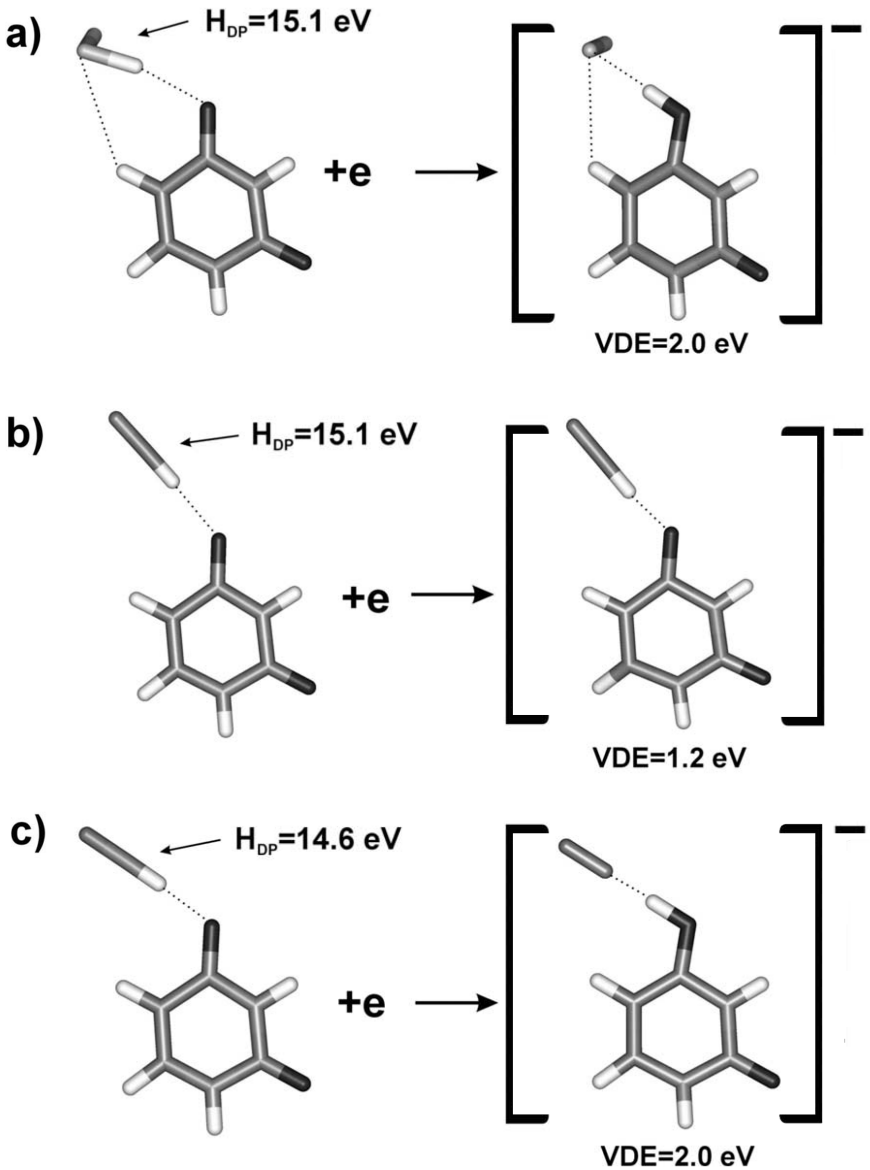

Fig. 2. The scheme of intermolecular hydrogen bonds in complexes of uracil with H_2S (a), HCN (b), and HNC (c).

broad feature with a maximum between 1.2 and 1.4 eV, whereas the main feature of the $(UH_2S)^-$ spectrum has a maximum between 1.7 and 2.1 eV. We suggest that the anionic complex of uracil with H_2S undergoes the intermolecular proton transfer, whereas the complex with HCN does not. In view of similar deprotonation enthalpies for HCN and H_2S, the difference is attributed to differences in hydrogen bonds formed by HCN and H_2S with uracil. We also predict that BFPT would occur in anionic complexes of uracil with HNC. The computational results presented in this study were obtained at the density functional theory level (DFT) with the B3LYP[40–42] and MPW1K[43] exchange-correlation functionals. In the case of HCN, which is a weak acid, stationary points on the potential energy surface were also explored at the second-order Møller-Plesset level of theory.

We describe our experimental and computational approaches in Section 2, with the photoelectron spectroscopy data for $(UHCN)^-$, as well as the calculated properties of the neutral and anionic complexes discussed in Section 3, and a summary in Section 4.

2. METHODS

2.1 Experimental

Negative ion photoelectron spectroscopy is conducted by crossing a mass-selected beam of negative ions with a fixed-frequency laser beam and energy-analyzing the resultant photodetached electrons.[44] It is governed by the energy-conserving relationship: hν = EBE + EKE, where hν is the photon energy, EBE is the electron binding energy, and EKE is the electron kinetic energy. One knows the photon energy of the experiment, one measures the electron kinetic energy spectrum, and then by difference, one obtains electron binding energies, which in effect are the transition energies from the anion to the various energetically-accessible states of its corresponding neutral.

Our apparatus has been described elsewhere.[45] To prepare the species of interest, uracil was placed in the stagnation chamber of a nozzle source and heated to ~180 °C. The expansion gas was a 5% HCN/argon mixture. Its total pressure was 1–2 atm., and the nozzle diameter was 25 μm. Electrons were injected into the emerging jet expansion from a biased Th/Ir filament in the presence of an axial magnetic field. The resulting anions were extracted and mass-selected with a magnetic sector mass spectrometer. Electrons were then photodetached from the selected anions with ~100 circulating watts of 2.540 eV photons and finally energy-analyzed with a hemispherical electron energy analyzer, having a resolution of 25 meV.

2.2 Computational

The notation $UHA_{x,y}$ and $aUHA_{x,y}$ will be used for the neutral and anionic complexes of uracil (U) and an acid (A = CN, NC, or SH), respectively. The symbol x stands for either the O8 or O7 atom of uracil, which is involved in a hydrogen bond with HA, while the symbol y indicates a side of the oxygen atom involved in the

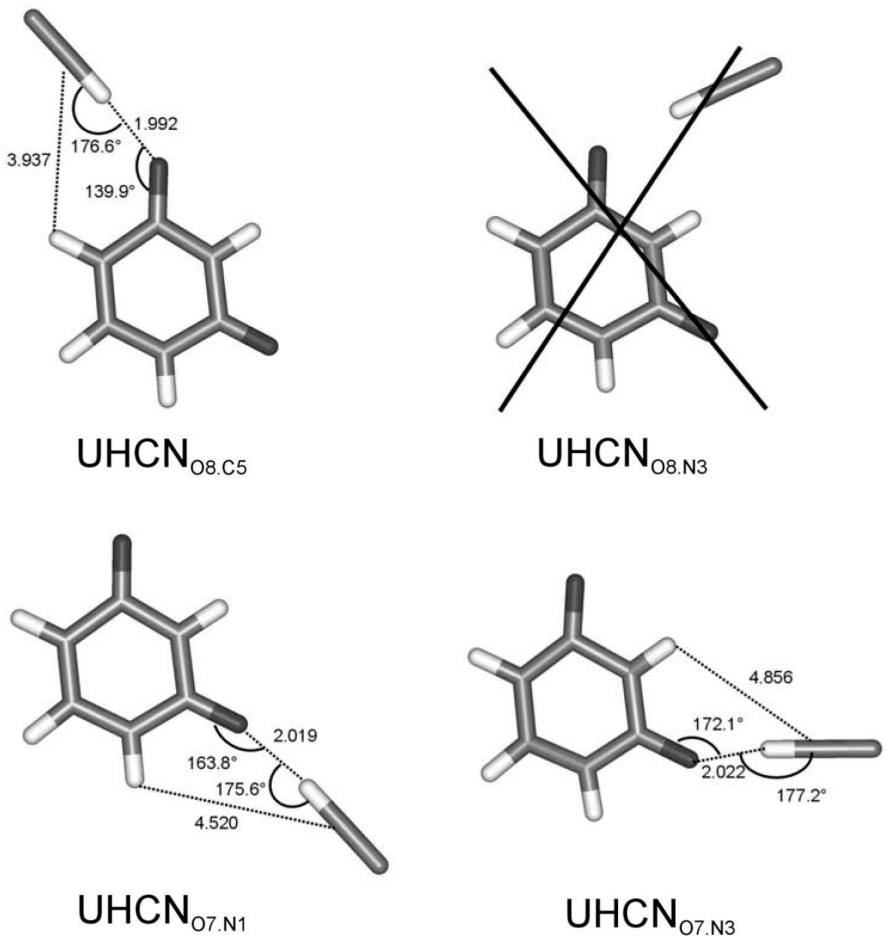

Fig. 3. The B3LYP/6-31++G** optimized structures of neutral UHCN complexes with the most important geometrical features. The $UHCN_{O8.N3}$ was not found (see text).

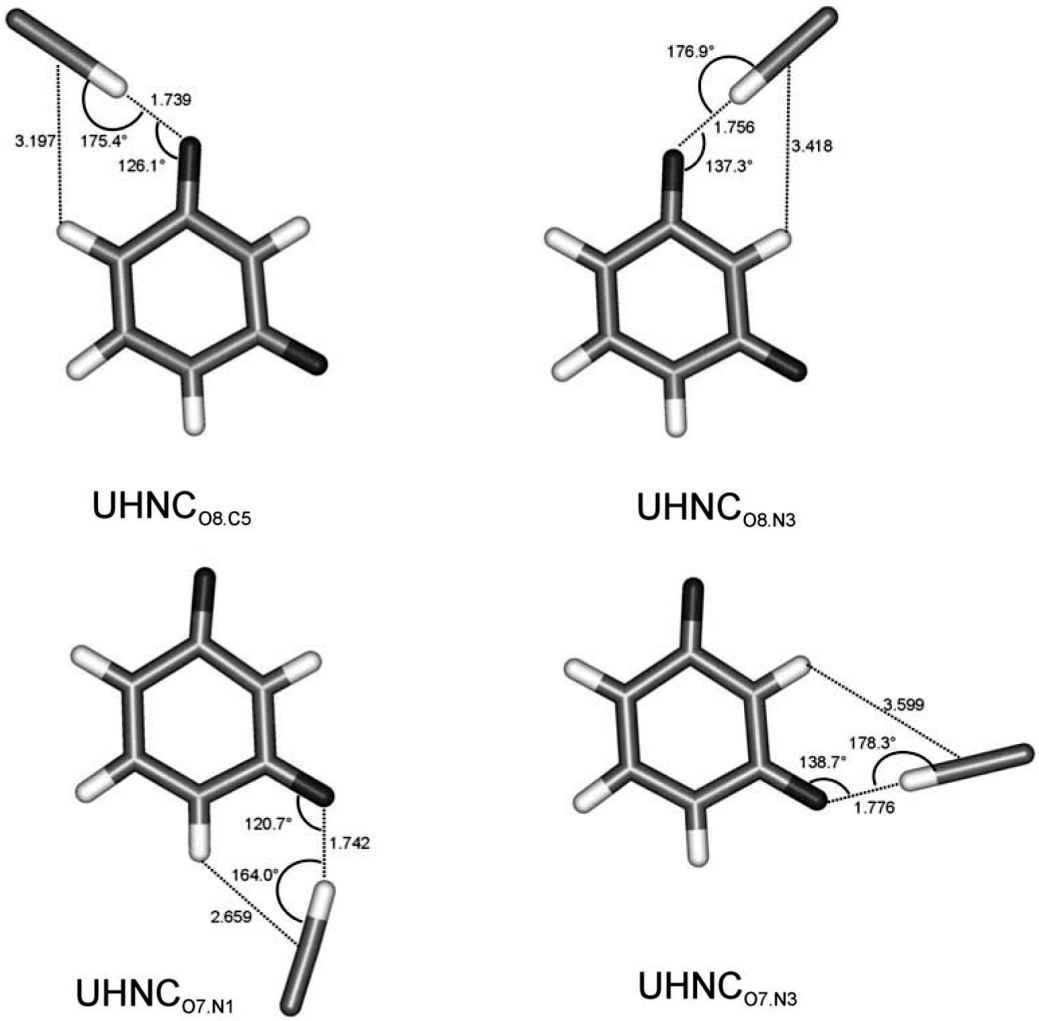

Fig. 4. The B3LYP/6-31++G** optimized structures of neutral UHNC complexes with the most important geometrical features.

hydrogen bond. Examples of this notation are presented in Figs. 3–6. Anionic minimum energy structures that have a (U^-…HA) and (UH…A^-) character will be denoted $aUHA_{x,y}$ and $aUHA_{x,y}$(PT), respectively (see Figs. 5 and 6), while transition states which separate the $aUHA_{x,y}$ and $aUHA_{x,y}$(PT) minima will be denoted $aUHA_{x,y}$(TS).

The stability of the neutral (superscript = 0) or anionic (superscript = –) UHA complexes is expressed in terms of E_{stab} and G_{stab}. E_{stab} is defined as a difference in electronic energies of the monomers and the dimer

$$E_{stab} = E^{U(0,-)}(Geom^{U(0,-)} + E^{HA}(Geom^{HA}) - E^{UHA(0,-)}(Geom^{UHA(0,-)}) \quad (2)$$

with the electronic energy E^X (X = $U^{(0,-)}$, HA, $UHA^{(0,-)}$) computed for the coordinates determining the optimal geometry of X (i.e., the geometry where E^X is at the minimum). The values of E_{stab} were not corrected for basis set superposition errors because our earlier results demonstrated that the values of this error in B3LYP/6-31++G** calculations for a similar neutral uracil-glycine complex did not exceed 0.06 eV.[46,47] The stabilization Gibbs energy, G_{stab}, results from supplementing E_{stab} with thermal contributions to energy from vibrations, rotations, and translations, pV terms, and the entropy term. The values of G_{stab} discussed below were obtained for T = 298 K and p = 1 atm, in the harmonic oscillator-rigid rotor approximation.

As our research method we applied density functional

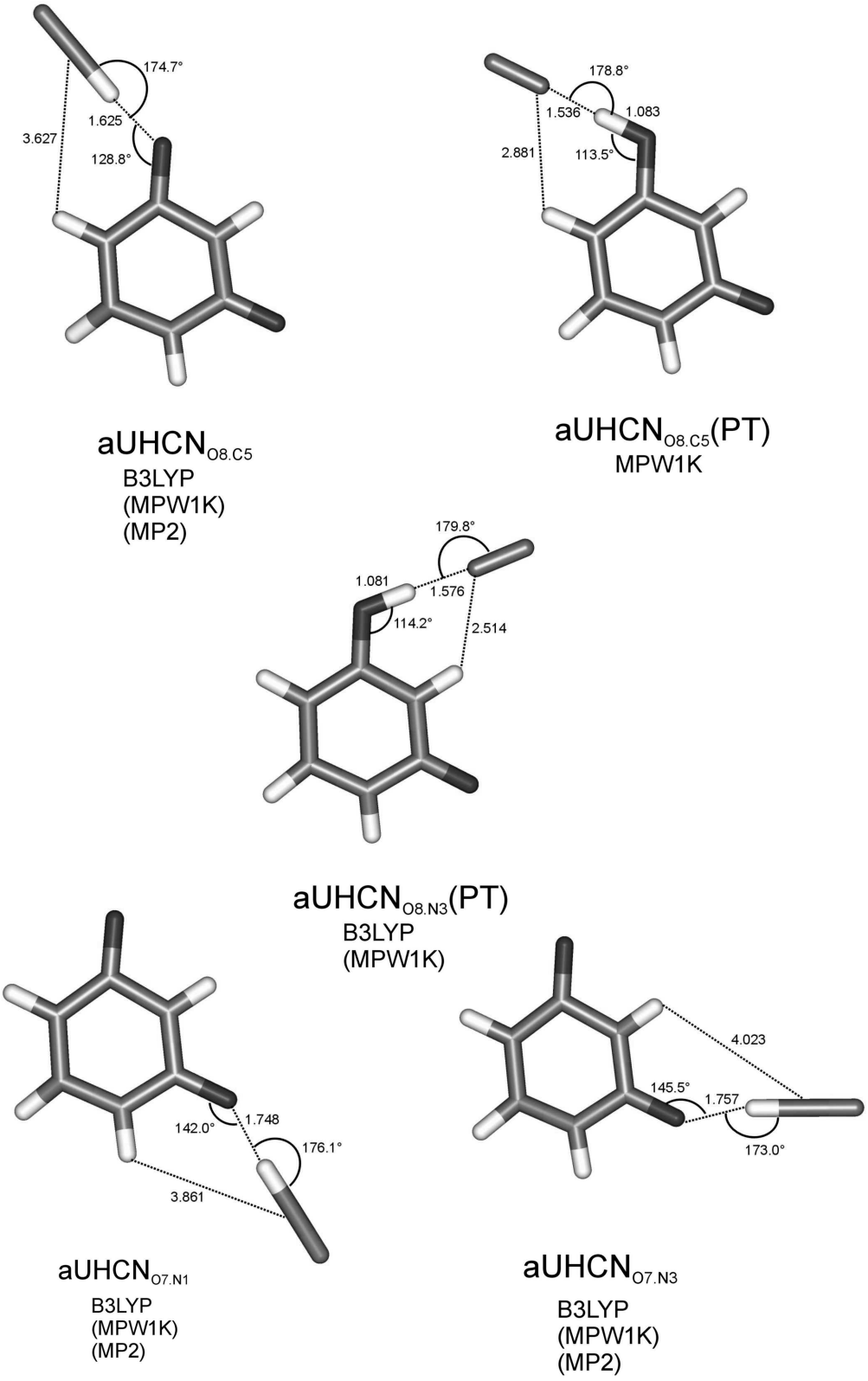

Fig. 5. The optimized structures of anionic UHCN complexes with the most important geometrical features. The aUHCN$_{O8.N3}$ was not found (see text).

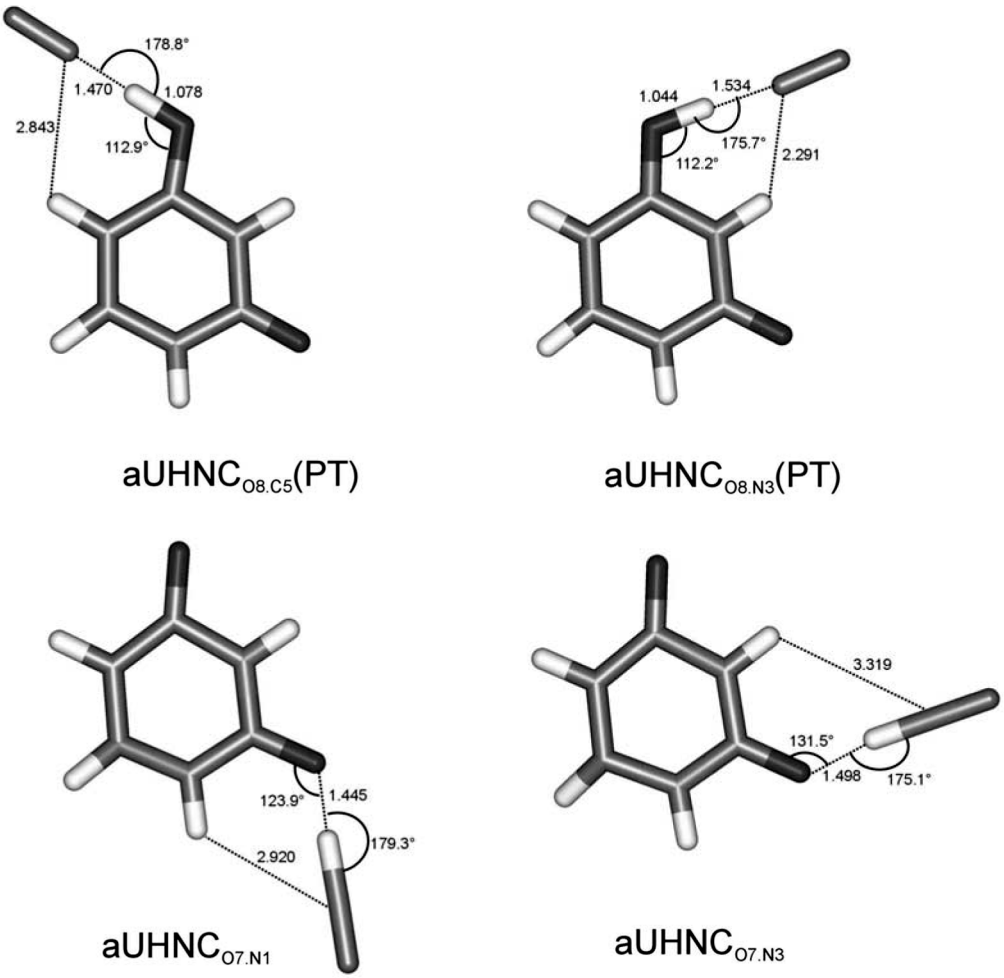

Fig. 6. The B3LYP/6-31++G** optimized structures of anionic UHNC complexes with the most important geometrical features.

theory with a Becke's three-parameter hybrid functional[40–42] (B3LYP) and a modified Perdew–Wang 1-parameter-method for kinetics (MPW1K) designed by Truhlar and coworkers.[42] In both DFT approaches we used the same 6-31++G** basis set.[48] Five d functions were used on heavy atoms. The calculations of matrices of second derivatives of energy (Hessians) were performed to confirm that final geometries were minima or transition states on potential energy surfaces.

The usefulness of the B3LYP/6-31++G** method to describe intra- and intermolecular hydrogen bonds has been demonstrated in recent studies through comparison with the second-order Møller-Plesset (MP2) predictions.[46,47,49,50,51] The ability of the B3LYP method to predict excess electron binding energies has recently been reviewed, and the results were found to be satisfactory for valence-type molecular anions.[52] A comparison with the CCSD(T)/aug-cc-pVDZ result suggests that the vertical detachment energy (VDE) for the valence π^* anionic state of an isolated uracil is overestimated by 0.2 and 0.3 eV at the B3LYP and MPW1K/6-31++G** level, respectively, and underestimated by 0.1 eV at the MP2/6-31++G** level. We will assume in the following that the same corrections of –0.2, –0.3, and +0.1 eV apply to the values of VDE at the B3LYP, MPW1K, and MP2 level, respectively, for all anionic UHA complexes in which an excess electron occupies a π^* orbital localized on uracil.

It is known that the B3LYP method underestimates barriers for proton transfer reactions, and thus, lack of a barrier may be an artifact of the B3LYP method. For this

reason, we performed additional geometry optimizations using a hybrid exchange-correlation potential MPW1K, which was parametrized to reproduce barrier heights for chemical reactions. The MPW1K functional was optimized against a database of 40 barrier heights and 20 energies of reaction.[43,53] It was suggested that the performance of this functional for geometries of saddle points and barrier heights might be superior to that of the B3LYP functional as well as the MP2 method.

The anionic complexes of uracil with HCN pose a challenge to DFT methods, as the presence of both the (U^-…HCN) and (UH…CN^-) minima on the potential energy surface is found to be sensitive to the selection of the exchange-correlation functional. In these cases we performed additional MP2/6-31++G** optimizations to verify existence of these minima. A spin contamination of the UHF wave function for the valence anion of uracil is not large as the value of S^2 is 0.793. The spin contamination is even smaller for anions described with the DFT wave functions.

All calculations were carried out with the GAUSSIAN 98 and NWChem[54] codes on a cluster of Intel/Xeon and Intel/Pentium3 nodes, a SGI Origin2000 numerical server, and an IBM SP.

3. RESULTS

3.1 PES Spectrum

The photoelectron spectrum of $(UHCN)^-$ is presented in Fig. 7 (middle) and compared to the spectra of $(UH_2O)^-$ (top, from ref 9) and (UH_2S) (bottom, from ref 35). The spectrum of $(UHCN)^-$ has a maximum at about 1.1–1.2 eV. The spectrum of $(UH_2O)^-$ is similar to that of $(UHCN)^-$, but its maximum is shifted to a smaller electron binding energy (ca. 0.9 eV). The spectrum of $(UH_2S)^-$ differs from the two and shows a broad and structureless feature with a maxima between 1.7–2.1 eV.

The valence π* and dipole-bound anionic states of uracil are characterized by a calculated value of VDE of 0.507 and 0.073 eV, respectively. Henceforth, only the valence π* anionic state will be considered further, since the experimental values of VDE for $(UHA)^-$ are far too large for the dipole-bound anionic state of U^- solvated by HA.

There is a clear resemblance in photoelectron spectra of $(UHCN)^-$ and $(UH_2O)^-$. We assume that the valence π* anionic state of uracil is involved in these spectra because the solvation of U^- by HCN or H_2O could easily stabilize U^- by the shifts seen in the spectra. The spectrum of $(UHCN)^-$ is shifted by about 0.2 eV to a higher value of electron binding energy in comparison to that of $(UH_2O)^-$. This may be explained by a stronger electrostatic stabilization of an excess electron localized on uracil in the former complex, as the dipole moment of HCN (3.05 D[55]) is larger than that of H_2O (1.86 D[56]).

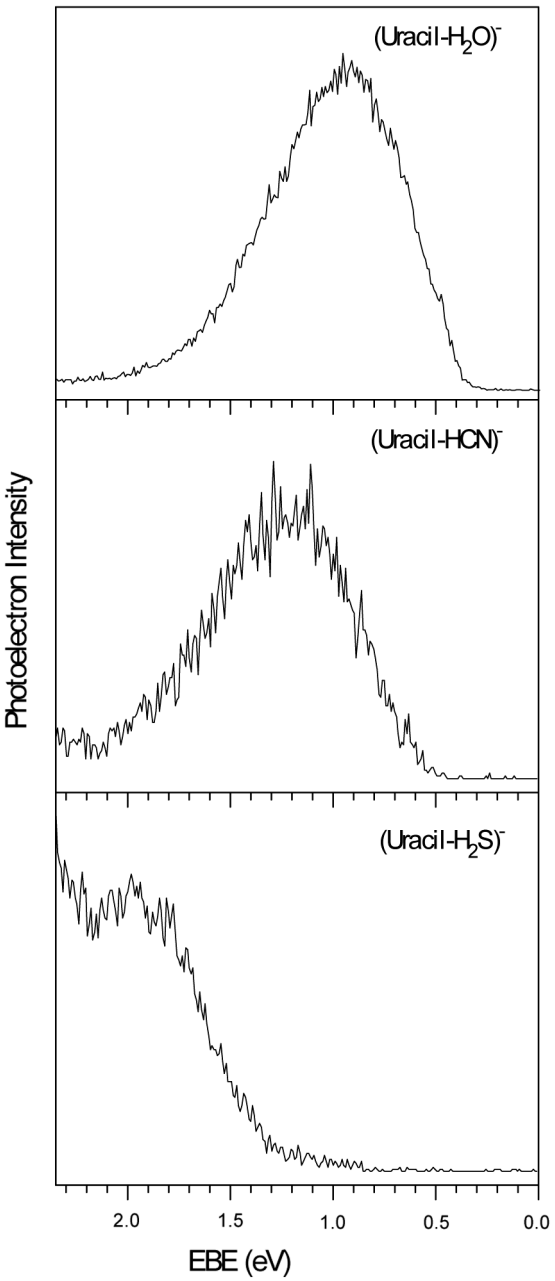

Fig. 7. Photoelectron spectra of uracil-H_2O dimer anion (top), uracil-HCN dimer anion (middle), and uracil-H_2S dimer anion (bottom) recorded with 2.540 eV/photon.

HCN and H_2S are characterized by very similar values of deprotonation enthalpy (H_{DP}), 15.217 ± 0.009[38] and 15.212 ± 0.126[39] eV, respectively. The spectra of their anionic complexes with uracil are, however, very

different. The result is surprising, as the values of H_{DP} suggest that HCN can be slightly more acidic than H_2S and thus more susceptible to intermolecular proton transfer in a complex with U^-. The experimental data suggest, however, that the proton transfer does not occur in $(UHCN)^-$. Thus, we conclude that the difference in the PES spectra results from the occurrence of intermolecular proton transfer in $(UH_2S)^-$, and lack thereof in $(UHCN)^-$. Moreover, we suggest that the occurrence of intermolecular proton transfer is controlled not only by the deprotonation enthalpy of the weak acid HA but also by the character of hydrogen bonds that develop in the $(UHA)^-$ complex.

3.2 Deprotonation Enthalpy of HA and Proton Affinity of U^-

The B3LYP, MPW1K, and MP2 values of deprotonation energies (E_{DP}), enthalpies (H_{DP}), and Gibbs free energies (G_{DP}) are presented in Table 1 for HNC, H_2S, and HCN and compared with the available experimental values.[38,39] The B3LYP/6-31++G** values of H_{DP} and G_{DP} for H_2S and HCN are within the experimental error bars, and the MP2/6-31++G** values are also very accurate. The MP2 results suggest that HCN is more acidic than H_2S, in agreement with the experimental data. The difference is less pronounced at the B3LYP level. For all systems, the calculated acidity is larger at the B3LYP than MP2 level of theory as the differences in the values of H_{DP} (or G_{DP}) can be as large as 0.2 eV. This suggests that the susceptibility to intermolecular proton transfer in anionic complexes with uracil will be larger at the B3LYP than MP2 level. The value of H_{DP} for HNC is smaller by ca. 0.5 eV than for HCN, hence HNC has a much larger propensity to intermolecular proton transfer with a basic agent than HCN.

We will concentrate on the O8 site of U^- because the results of our previous studies[20,35,36,37] suggest that the O7 site is much more resistant to intermolecular proton transfer. The B3LYP, MPW1K, and MP2 values of protonation energy (E_P), enthalpy (H_P), and Gibbs free energy (G_P) for the C5 and N3 sides of the O8 site of U^- are presented in Table 2. The protonation is more favorable on the C5 than N3 side by a few hundredths of an electronvolt. The B3LYP and MP2 values of E_P are the same to within 0.02 eV, while the MPW1K values are larger by 0.23 eV. These data suggest that the susceptibility of U^- to intermolecular proton transfer in complexes with weak acids will be the largest at the MPW1K level but similar at the B3LYP and MP2 levels.

3.3 Neutral Complexes

The HCN, HNC, and H_2S form a series of nonoxyacids with different preferences for hydrogen bonding. HCN and HNC can engage only one site, i.e., a proton donor, in a strong hydrogen bond with uracil (see Figs. 2b,c, 3, and 4). Formally, they can also engage their central atom in a hydrogen bond with a proton donor of U. Indeed, HNC can form an additional but weak hydrogen bond with uracil. The second hydrogen bond is practically nonexistent in a complex of HCN with U, as the C atom is not a sufficiently strong proton acceptor. H_2S, on the other hand, can form two strong hydrogen bonds with its SH and a lone electron pair of S acting as a proton donor and acceptor, respectively (see Fig. 2a). A detailed characteristic of the neutral and anionic UH_2S complexes was provided in ref 35.

The neutral complexes UHA (A = CN, NC) can be formed with HA coordinated to either side of uracil's O8 or O7 proton-accepting sites. Hence, the topological space is limited to four important structures; see Figs. 3 and 4 where the important geometrical parameters are also presented. In Table 3 we present the energies of

Table 1. The calculated deprotonation energy (E_{DP}), enthalphy (H_{DP}), and Gibbs free energy (G_{DP}) of HA. All results in eV. The result obtained at different level of theory using 6-31++G** basis sets

acid	method	E_{DP}	H_{DP}	G_{DP}	H_{DP}^{exp}	G_{DP}^{exp}
HNC	B3LYP	14.806	14.561	14.230		
	MPW1K	14.965	14.710	14.378		
	MP2	14.693	14.441	14.111		
H_2S	B3LYP	15.313	15.115	14.838	15.212 ± 0.126*	14.935 ± 0.130*
	MPW1K	15.424	15.217	14.922		
	MP2	15.529	15.318	15.023		
HCN	B3LYP	15.382	15.129	14.789	15.217 ± 0.009**	14.935 ± 0.130**
	MPW1K	15.497	15.233	14.892		
	MP2	15.478	15.230	14.891		

* ref 39.
** ref 38.

Table 2. The calculated protonation energy (E_P), enthalpy (H_P), and Gibbs free energy (G_P) of U^- at the O8 site at different levels of theory. All results in eV. All values obtained with 6-31++G** basis sets

side	method	E_P	H_P	G_P
C5 Side	B3LYP	14.697	14.410	14.099
	MPW1K	14.927	14.632	14.316
	MP2	14.683	14.198	13.876
N3 Side	B3LYP	14.650	14.367	14.034
	MPW1K	14.876	14.585	14.262
	MP2	14.669	14.145	13.813

Table 3. Thermodynamic characteristics of the neutral complexes. All results obtained with 6-31++G** basis sets. The MP2 values of E_{stab} were supplemented with zero-point vibration energy (ZPVE) as well as thermal corrections to G_{stab} determined at the B3LYP level. All energies in eV

complex	method	E_{stab}	E_{stab}+ZPVE	G_{stab}
$UHCN_{O8.C5}$	B3LYP	0.271	0.231	–0.063
	MP2	0.288	0.248	–0.045
$UHCN_{O7.N1}$	B3LYP	0.239	0.204	–0.076
	MP2	0.261	0.227	–0.020
$UHCN_{O7.N3}$	B3LYP	0.238	0.204	–0.042
	MP2*			
$UHNC_{O8.C5}$	B3LYP	0.421	0.361	0.020
$UHNC_{O8.N3}$	B3LYP	0.388	0.330	0.003
$UHNC_{O7.N1}$	B3LYP	0.387	0.332	–0.016
$UHNC_{O7.N3}$	B3LYP	0.361	0.305	–0.018

*The MP2 geometry optimization converged to the $UHCN_{O7.N1}$ structure.

stabilization, energies corrected for zero-point vibration energies, as well as Gibbs free energies for the neutral complexes.

There is an important difference in preferable geometries of the UHA (A = CN, NC) and UH_2S complexes. The former favors the O8C5 geometry, i.e., HA is coordinated to the O8 atom from the C5 side. The latter favors the O7N1 geometry, which is typical for complexes of uracil with ligands, which provide both proton donor and acceptor sites.[46,47] In the case of the UHCN and UHNC complexes, only a proton acceptor site of U matters, and it is the most basic for the C5 side of O8. Thus, the O8C5 geometry is the most favorable. In the case of UH_2S, both the proton donor and acceptor sites of U matter. The N1H site of uracil is the most acidic and this justifies the largest stability of UH_2S complexes for the O7N1 geometry.

The UHCN and UHNC complexes differ due to the second hydrogen bond, which is weak but operational for the latter and probably negligible for the former. For instance, for the O8C5 complexes, a difference of 0.7 Å between the C5H…CN and C5H…NC distances confirms that N in HNC is a much better "proton acceptor" than C in HCN (see Figs. 3 and 4). Similar results are found for the O7 bonded complexes. Because of the lack of stabilization due to the second hydrogen bond, the $UHCN_{O8.N3}$ minimum does not exist on the potential energy surface and the geometry optimization procedure collapses to the $UHCN_{O8.C5}$ structure. For UHNC, however, both minima exist, with the $UHNC_{O8.C5}$ structure being more stable.

All complexes but $UHNC_{O8.X}$ (X = C5, N3) are unstable in terms of Gibbs free energy (see Table 3). It requires an E_{stab} larger than 0.39 eV to favor formation, i.e., a positive value of G_{stab}, of a neutral UHNC complex in the gas phase. The stabilization energies for the UHCN complexes determined at the MP2 level are only ca. 0.02 eV larger than those determined with the B3LYP exchange-correlation functional. This gives us some confidence as to the consistency of theoretical predictions.

3.4 Anionic complexes

A common feature of anionic wave functions identified by us for the UHA complexes is that the excess electron is localized on a π^* orbital of uracil, in close resemblance to the valence anionic state of isolated uracil (see Figs. 1 and 8). An isolated uracil molecule has a symmetry plane. However, occupation of the antibonding π^* orbital by an excess electron in isolated uracil induces buckling of the ring because non-planar structures are characterized by a less severe antibonding interaction. The same kind of ring distortion takes place in all UHA complexes upon an excess electron attachment.

Anionic complexes of U with HCN pose a challenge to theoretical models as the acidity of HCN makes the intermolecular proton transfer plausible, though its occurrence also requires favorable hydrogen bonding interactions. The properties of anionic UHCN complexes were determined with the B3LYP and MPW1K exchange-correlation functionals as well as at the MP2 level of theory. The structures of the most important stationary points are displayed in Fig. 5 and the thermodynamic characteristics are collected in Table 4.

A comparison of the photoelectron spectrum (see Fig. 7) and computational data (Table 4) suggests that $(UHCN)^-$ does not undergo the intermolecular proton transfer. Hence, the global minimum corresponds to the U^-…HCN complex. A position of the broad maximum of the photoelectron spectrum at 1.1–1.2 eV, and the estimated values of electron vertical detachment energies

Table 4. Thermodynamic characteristics of the anionic complexes. All results obtained with 6-31++G** basis sets. The MP2 values of E_{stab} were supplemented with zero-point vibration energy (ZPVE) as well as thermal corrections to G_{stab} determined at the B3LYP level. All energies in eV

complex	method	E_{stab}	E_{stab}+ZPVE	G_{stab}	VDE*
$aUHCN_{O8.C5}$	B3LYP	0.883	0.854	0.533	1.2
	MPW1K	0.945	0.921	0.598	1.2
	MP2	0.857	0.828	0.492	1.1
$aUHCN_{O8.C5}$(PT)	MPW1K	0.865	0.866	0.507	1.9
$aUHCN_{O8.C5}$(TS)	MPW1K	0.861	0.927	0.557	
$aUHCN_{O8.N3}$(PT)	B3LYP	0.708	0.691	0.326	2.0
	MPW1K	0.835	0.803	0.436	2.0
$aUHCN_{O8.N3}$(TS)	B3LYP	0.702	0.759	0.384	
	MPW1K	0.798	0.868	0.496	
$aUHCN_{O7.N1}$	B3LYP	0.690	0.651	0.337	1.0
	MP2	0.670	0.631	0.317	0.9
$aUHCN_{O7.N3}$	B3LYP	0.689	0.649	0.327	1.0
	MP2	0.665	0.624	0.303	0.9
$aUHNC_{O8.C5}$(PT)	B3LYP	1.308	1.270	0.905	2.0
$aUHNC_{O8.N3}$(PT)	B3LYP	1.307	1.244	0.867	2.0
$aUHNC_{O7.N1}$	B3LYP	0.971	0.937	0.575	1.2
$aUHNC_{O7.N3}$	B3LYP	0.944	0.900	0.546	1.2

* The B3LYP, MPW1K, and MP2 values of VDE were corrected for –0.2, –0.3, and +0.1 eV, respectively; see Section 2 for details.

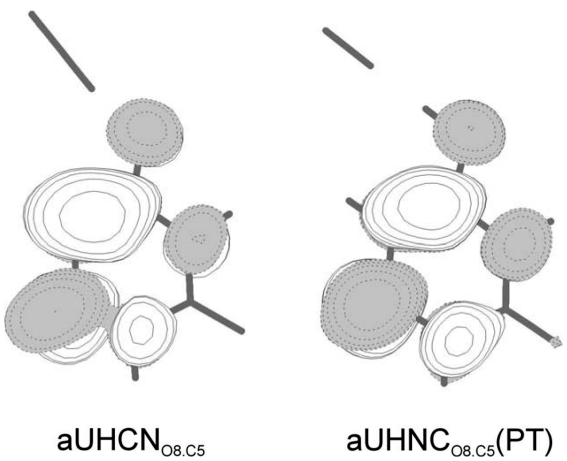

Fig. 8. The SOMO orbital in $aUHCN_{O8.C5}$ and $aUHNC_{O8.C5}$ obtained with B3LYP/6-31++G**. The orbital was plotted with a contour line spacing of 0.03 bohr$^{-3/2}$.

(VDE) for the global minimum, which are 1.1 and 1.2 eV at the MP2 and B3LYP level, respectively, are consistent, thus confirming the main finding.

The interpretation is straightforward at the MP2 level of theory, for which only the U$^-$…HCN minima, …HCN minima, i.e., 08.C5, 07.N1, 07.N3, have been identified (see Table 4). It should be noticed, however, that DFT theoretical models predict existence of local minima on the anionic potential energy surface that correspond to a UH…CN$^-$ complex. The estimated values of VDE for such minima are 1.9–2.0 eV, hence larger by 0.7–0.8 eV than for the most stable U$^-$…HCN structure. If the UH…CN$^-$ structures were populated in the anionic beam, their presence would be reflected in the photoelectron spectrum. These local minima are less stable than the global minimum by 1.8–4.2 kcal/mol. Moreover, a MPW1K barrier that separates the local minimum $aUHCN_{O8.C5}$(PT) from the global minimum is only 0.004 eV. In addition, the barrier disappears on the Gibbs free energy surface. Analogous pattern is observed for the $aUHCN_{O8.N3}$ structure at the B3LYP theory level. We suspect that the UH…CN$^-$ minima on the DFT potential energy surfaces are artifacts of the computational models because the VDE for U$^-$ is overestimated by 0.2 (B3LYP) and 0.3 (MPW1K) eV. Even if the anionic PT-type minima are genuine, the absence of a significant feature in the photoelectron spectrum at the 1.8–2.1 eV range demonstrates that they must be relatively unstable with respect to the global $aUHCN_{O8.C5}$ minimum.

The largest susceptibility of (UHCN)$^-$ to proton transfer with the MPW1K functional can be traced back to a large value of E_p for U$^-$ (see Table 2). The largest

resistance to proton transfer at the MP2 level of theory can be traced back to a large value of E_{DP} for HCN and a small value of E_P for U^- (see Tables 1 and 2).

Next, let us turn to the anionic UHNC complexes. A small deprotonation energy of HNC facilitates occurrence of BFPT in some $(UHNC)^-$ complexes (see Table 4 and Fig. 6). The BFPT occurs in these anionic complexes in which HNC is coordinated to the O8 site. A driving force for the proton transfer is to stabilize the excess negative charge, which is primarily localized in the O8–C4–C5–C6 region (see Figs. 1 and 8). In consequence of the extra stabilization of the excess electron provided by the transferred proton, the values of VDE for $aUHNC_{O8.C5}$ and $aUHNC_{O8.N3}$ are as large as 2.0 eV. The proton affinity of U^- at the O7 site is too small to support an anionic PT-type structure. The excess electron of U^- is not localized in the neighborhood of O7 (see Fig. 1). This explains why coordination of HNC to any side of O7 is not followed by BFPT and the values of VDE for the resulting complexes $aUHNC_{O7.N1}$ and $aUHNC_{O7.N3}$ are estimated to be only 1.2 eV.

The relative stability of different structures for both the $(UHCN)^-$ and $(UHNC)^-$ complexes correlates with the value of proton affinity of this site of U^-, which is involved in the hydrogen bond (see Tables 2 and 4). More stable anionic complexes with uracil are formed when either HNC or HCN is coordinated to the O8 rather than to the O7 site. Moreover, the C5 side of O8 is more favorable than the N3 side. In contract, the H_2S ligand, which undergoes BFPT in anionic complexes with uracil, favors the O8N3 binding site because the quality of both hydrogen bonds matters for a cyclic hydrogen bonded structure.

The anionic O7N1 and O7N3 complexes undergo BFPT neither with HCN nor with HNC. The geometric characteristics of hydrogen bonds are, however, different depending on whether HCN or HNC is involved. The strong bond is shorter by 0.25–0.30 Å for complexes with HNC, which might reflect the fact that dipole moment is larger by ca. 0.2 D for HNC than for HCN. The second hydrogen bond is weak but operational in complexes with HNC and probably negligible in complexes with HCN. For instance for the O7N1 complexes, a difference of 0.9 Å between the N1H...CN and N1H...NC distances confirms that N in HNC is a much better "proton acceptor" than C in HCN (see Figs. 5 and 6).

The occurrence of BFPT in $(UH_2S)^-$ and lack thereof in $(UHCN)^-$ is intriguing, as the deprotonation energy is very similar for H_2S and HCN. The products of the intermolecular proton transfer would be the neutral radical $UH^\cdot$ and A^-. For further analysis, we will use the MP2 values of E_{DP} and E_P for HAs and U^-, respectively (see Tables 1 and 2). The largest value of E_P for U^- is reported at the O8 site (C5 side) and amounts to 14.68 eV. Hence, a hypothetical process, which leads to noninteracting products

$$HA + U^- \rightarrow A^- + UH^\cdot \qquad (3)$$

is unfavorable in terms of energy by 0.80, 0.85, and 0.01 eV for HCN, H_2S, and HNC, respectively. For the proton transfer to occur, the stabilizing interaction in the $UH^\cdot...A^-$ system needs to (i) compensate the aforementioned barrier and (ii) provide additionally at least as much of the stabilization between the $UH^\cdot$ and A^- systems as the untransformed U^- and HA moieties could provide. The barrier is smaller for HCN than for H_2S, but the proton transfer occurs for the latter but not for the former. We conclude that the hydrogen bonding in $(UHCN)^-$ fails to provide as much stabilization as in $(UH_2S)^-$. A general conclusion that came out of this analysis is that the occurrence of intermolecular proton transfer results from a subtle interplay between the deprotonation energy of HA, protonation energy of U^-, and the intermolecular stabilization energy.

4. SUMMARY

The photoelectron spectrum of the anionic uracil–HCN complex has been recorded with 2.540 eV photons. The spectrum reveals a broad feature with its maximum between EBE = 1.1–1.2 eV. The vertical electron detachment energy value is larger than in the $(UH_2O)^-$ complex, but the $(UHCN)^-$ complex can still be interpreted as U^- solvated by HCN. On the other hand, the spectrum of $(UHCN)^-$ is different from the recently recorded spectrum of the anionic uracil–H_2S complex, for which a barrier-free proton transfer was suggested from H_2S to the O8 atom of anionic uracil.

The results of density functional calculations with the B3LYP and MPW1K exchange-correlation functionals and at the MP2 level of theory indicate that an excess electron in the UHA (A = NC, CN) complexes is described by a π^* orbital localized on the ring of uracil. The ring is buckled because nonplanar structures are characterized by a less severe antibonding interaction.

A comparison of the photoelectron spectrum and computational data confirms that $(UHCN)^-$ does not undergo the intermolecular proton transfer. Indeed, the global minimum corresponds to the $U^-…HCN$ complex. A position of the broad maximum of the photoelectron spectrum at 1.1–1.2 eV, and the estimated values of electron vertical detachment energies for the global minimum, which are 1.1 and 1.2 eV at the MP2 and B3LYP level, respectively, are consistent, thus confirming the main finding.

The occurrence of BFPT in $(UH_2S)^-$ and lack thereof

in $(UHCN)^-$ is intriguing, as the deprotonation energy is very similar for H_2S and HCN. We demonstrate, however, that the hydrogen bonding in $(UHCN)^-$ fails to provide as much stabilization as in $(UH_2S)^-$. The occurrence of intermolecular proton transfer results from a subtle interplay between the deprotonation energy of HA, protonation energy of U^-, and the intermolecular stabilization energy. A small variation in any of these parameters can alter the $U^-\ldots HA \leftrightarrow UH\ldots A^-$ equilibrium. Such variations are indeed observed among the computational methods used.

The computational results indicate that a small deprotonation energy of HNC facilitates occurrence of BFPT in some $(UHNC)^-$ complexes. A driving force for the proton transfer is to stabilize the excess negative charge, which is primarily localized in the O8–C4–C5–C6 region. Thus, the intermolecular proton transfer occurs from HNC to the O8 site of uracil. The calculated values of VDE for $aUHNC_{O8.C5}$ and $aUHNC_{O8.N3}$ are as large as 2.0 eV.

For neutral complexes, the favorable sites of U to bind HCN or HNC are different than those in complexes with H_2S. The first two complexes favor the O8C5 geometry. The latter favors the O7N1 geometry, which is typical for complexes of uracil with ligands, which provide both proton donor and acceptor sites. In the case of the UHCN and UHNC complexes, only a proton acceptor site of U matters, and it is the most basic for the C5 side of O8. In the case of UH_2S, both the proton donor and acceptor sites of U matter. The N1H site of uracil is the most acidic, and this justifies the largest stability of UH_2S complexes for the O7N1 geometry.

An important issue for future experimental and theoretical studies is to characterize the propensity of cytosine and thymine to BFPT in anionic complexes with inorganic and organic acids. Lastly, the formation of neutral radicals of hydrogenated pyrimidine bases may be relevant to DNA and RNA damage by low-energy electrons. For instance, the neutral radical $UH^{\cdot}$ (and probably thymine-$H^{\cdot}$), with the O8 atom protonated, cannot form a hydrogen bond with adenine, as dictated by the Watson–Crick pairing scheme. An anion of $UH^{\cdot}$ radical might also react with an adjacent deoxyribose molecule triggering strand breaks in DNA.[57]

Acknowledgments. This work was supported by the: (i) US DOE OBER, Low Dose Radiation Research Program (M.H. and M.G.), (ii) NSF grant CHE-0211522 (K.B.), (iii) Polish State Committee for Scientific Research (KBN) Grant KBN 4 T09A 012 24 (J.R.). The calculations were performed at the National Energy Research Scientific Computing Center (NERSC) and at the Academic Computer Center in Gdansk (TASK). Pacific Northwest National Laboratory is operated by Battelle for the U.S. DOE under Contract DE-AC06-76RLO 1830.

REFERENCES AND NOTES

(1) Michael, B.R.; O'Neill, P. *Science* **2000**, *287*, 1603–1604.
(2) Burrows, C.J.; Muller, J.G. *Chem. Rev.* **1998**, *98*, 1109–1152.
(3) Armitage, B. *Chem. Rev.* **1998**, *98*, 1171–1200.
(4) Boudaïffa, B.; Cloutier, P.; Hunting, D.; Huels, M.A.; Sanche, L. *Science* **2000**, *287*, 1658–1660.
(5) Sanche, L. *Mass Spectrom. Rev.* **2002**, *21*, 349–369.
(6) Miller, J.H.; Wilson, W.W.; Ritchie, R.H. In *Computational Approaches in Molecular Radiation Biology*; Varma, M.N.; Chatterjee, A., Eds.; Plenum Press: New York, 1995; pp 65–76.
(7) Barrios, R.; Skurski, P.; Simons, J. *J. Phys. Chem. A* **2002**, *106*, 7991–7994.
(8) Desfrancois, C.; Carles, S.; Schermann, J.P. *Chem. Rev.* **2000**, *100*, 3943–3962.
(9) Hendricks, J.H.; Lyapustina, S.A.; deClercq, H.L.; Bowen, K.H. *J. Chem. Phys.* **1998**, *108*, 8–11.
(10) Weinkauf, R.; Schermann, J.-P.; de Vries, M.S. *Eur. Phys. J. D* **2002**, *20*, 309–316 and references therein.
(11) Oyler, N.A.; Adamowicz, L. *J. Phys. Chem.* **1993**, *97*, 11122–11123.
(12) Oyler, N.A.; Adamowicz, L. *Chem. Phys. Lett.* **1994**, *219*, 223–227.
(13) Gutowski, M.; Skurski, P. *Recent Res. Dev. Phys. Chem.* **1999**, *3*, 245–260.
(14) Dolgounitcheva, O.; Zakrzewski, V.G.; Ortiz, J.V. *Chem. Phys. Lett.* **1999**, *307*, 220–226.
(15) Dolgounitcheva, O.; Zakrzewski, V.G.; Ortiz, J.V. *J. Phys. Chem. A* **1999**, *103*, 7912–7917.
(16) Gutowski, M.; Skurski, P.; Simons, J. *J. Am. Chem. Soc.* **2000**, *122*, 10159–10162.
(17) Skurski, P.; Rak, J.; Simons, J.; Gutowski, M. *J. Am. Chem. Soc.* **2001**, *123*, 11073–11074.
(18) Rak, J.; Skurski, P.; Gutowski, M. *J. Chem. Phys.* **2001**, *114*, 10673–10681.
(19) Wesolowski, S.S.; Leininger, M.L.; Pentchev, P.N.; Schaefer, H.F., III. *J. Am. Chem. Soc.* **2001**, *123*, 4023–4028.
(20) Gutowski, M.; Dąbkowska, I.; Rak, J.; Xu, S.; Nilles, J.M.; Radisic, D.; Bowen, K.H., Jr. *Eur. Phys. J. D* **2002**, *20*, 431–439.
(21) Sevilla, M.D.; Besler, B.; Colson, A.O. *J. Phys. Chem.* **1995**, *99*, 1060–1063.
(22) Lowdin, P.O. *Rev. Mod. Phys.* **1963**, *35*, 724–732.
(23) Estrin, D.A.; Paglieri, L.; Corongiu, G. *J. Phys. Chem.* **1994**, *98*, 5653–5660.
(24) Morpugo, S.; Bossa, M.; Morpugo, G.O. *Chem. Phys. Lett.* **1997**, *280*, 233–238.
(25) Kryachko, E.S.; Nguyen, M.T.; Zeegers-Huyskens, T. *J. Phys. Chem. A* **2001**, *105*, 1288–1295.
(26) Kryachko, E.S.; Nguyen, M.T.; Zeegers-Huyskens, T. *J. Phys. Chem. A* **2001**, *105*, 1934–1943.
(27) Hobza, P.; Sponer, J. *Chem. Rev.* **1999**, *99*, 3247–3276.
(28) Dąbkowska, I.; Gutowski, M.; Rak, J. Submitted to *J. Am. Chem. Soc.*
(29) Kim, Y.; Lim, S.; Kim, Y. *J. Phys. Chem. A* **1999**, *103*,

6632–6637.
(30) Bertran, J.; Olivia, A.; Rodriguez-Santiago, L.; Sodupe, M. *J. Am. Chem. Soc*. **1998**, *120*, 8159–8167.
(31) Takeuchi, S.; Tahara, T. *Chem. Phys. Lett.* **1997**, *277*, 340–346.
(32) Zhanpeisov, N.U.; Sponer, J.; Leszczynski, J. *J. Phys. Chem. A* **1998**, *102*, 10374–10379.
(33) He, F.; Ramirez, J.; Lebrilla, C.B. *J. Am. Chem. Soc.* **1999**, *121*, 4726–4727.
(34) Li, X.; Cai, Z.; Sevilla, M.D. *J. Phys. Chem. A* **2001**, *106*, 9345–9351.
(35) Haranczyk, M.; Bachorz, R.; Rak, J.; Gutowski, M.; Nilles, J.M.; Stokes, S.T.; Radisic, D.; Bowen, K.H., Jr. *J. Phys. Chem. B* **2003**, *107*, 7889–7895.
(36) Dąbkowska, I.; Rak, J.; Gutowski, M.; Nilles, J.M.; Radisic, D.; Bowen, K.H., Jr. *J. Chem. Phys* **2004**, *120*, 6064–6071.
(37) Haranczyk, M.; Dąbkowska, I.; Rak, J.; Gutowski, M.; Nilles, J.M.; Stokes, S.T.; Radisic, D.; Bowen, K.H., Jr. *J. Phys. Chem. B* **2004**, *108*, 6919–6921.
(38) Bradforth, S.E.; Kim, E.H.; Arnold, D.W.; Neumark, D.M. *J. Chem. Phys.* **1993**, *98*, 800–810.
(39) Rempala, K.; Ervin, K.M. *J. Chem. Phys.* **2000**, *112*, 4579–4590.
(40) Becke, A.D. *Phys. Rev. A* **1988**, *38*, 3098–3100.
(41) Becke, A.D. *J. Chem. Phys.* **1993**, *98*, 5648–5652.
(42) Lee, C.; Yang, W.; Paar, R.G. *Phys. Rev. B* **1988**, *37*, 785–789.
(43) Lynch, B.J.; Fast, P.L.; Harris, M.; Truhlar, D.G. *J. Phys. Chem. A* **2000**, *104*, 4811–4815.
(44) Coe, J.V.; Snodgrass, J.T.; Freidhoff, C.B.; McHugh, K.M.; Bowen, K.H. *J. Chem. Phys.* **1987**, *87*, 4302–4309.
(45) Coe, J.V.; Snodgrass, J.T.; Freidhoff, C.B.; McHugh, K.M.; Bowen, K.H. *J. Chem. Phys*. **1986**, *84*, 618–625.
(46) Dąbkowska, I.; Rak, J.; Gutowski, M. *J. Phys. Chem. A* **2002**, *106*, 7423–7433.
(47) Dąbkowska, I.; Gutowski, M.; Rak, J. *Pol. J. Chem.* **2002**, *76*, 1243–1247.
(48) Frisch, M.J. et al. Gaussian, Inc., Pittsburgh, PA, 1998.
(49) Rak, J.; Skurski, P.; Simons, J.; Gutowski, M. *J. Am. Chem. Soc*. **2001**, *123*, 11695–11707.
(50) van Mourik, T.; Price, S.L.; Clary, D.C. *J. Phys. Chem. A* **1999**, *103*, 1611–1618.
(51) Dkhissi, A.; Adamowicz, L.; Maes, G. *J. Phys. Chem. A* **2000**, *104*, 2112–2119.
(52) Rienstra-Kiracofe, J.C.; Tschumper, G.S.; Schaefer, H.F., III. *Chem. Rev.* **2002**, *102*, 231–282.
(53) Lynch, B.J.; Truhlar, D.G. *J. Phys. Chem. A* **2001**, *105*, 2936–2941.
(54) Harrison, R.H., et al. 2001. NWChem, A Computational Chemistry Package for Parallel Computers, Version 4.0.1, 2001.
(55) Peterson, K.A.; Gutowski, M. *J. Chem. Phys.* **2002**, *116*, 3297–3299.
(56) Pauling, L. *General Chemistry*; Dover: New York, 1988; p 180.
(57) Dąbkowska, I. et al. In preparation.